Trapping wave fields in an expulsive potential by means of linear coupling

Nir Hacker[1] and Boris A. Malomed [1,2]

[1]*Department of Physical Electronics, School of Electrical Engineering, Faculty of Engineering, and Center for Light-Matter interaction, Tel Aviv University, Tel Aviv 69978, Israel*

[2]*Instituto de Alta Investigación, Universidad de Tarapacá, Casilla 7D, Arica, Chile*

We demonstrate the existence of confined states in one- and two-dimensional (1D and 2D) systems of two linearly coupled components, with the confining harmonic-oscillator (HO) potential acting upon one component and an expulsive anti-HO potential acting upon the other. The systems can be implemented in optical and BEC dual-core waveguides. In the 1D linear system, codimension-one solutions are found in an exact form for the ground state (GS) and dipole mode (the first excited state). Generic solutions are produced by means of the variational approximation and are found in a numerical form. Exact codimension-one solutions and generic numerical ones are also obtained for the GS and vortex states in the 2D system (the exact solutions are found for all values of the vorticity). Both the trapped and antitrapped components of the bound states may be dominant ones, in terms of the norm. The localized modes may be categorized as *bound states in continuum*, as they coexist with delocalized ones. The 1D states, as well as the GS in 2D, are weakly affected and remain stable if the self-attractive or repulsive nonlinearity is added to the system. The self-attraction makes the vortex states unstable against splitting, while they remain stable under the action of the self-repulsion.

I. INTRODUCTION

The combination of the harmonic-oscillator (HO) trapping potential and cubic nonlinearity is a ubiquitous setting which occurs in diverse physical realizations. A well-known one is offered by Bose-Einstein condensates (BECs) with the mean-field nonlinearity [1–3], loaded in a magnetic or optical trap—see, e.g., Refs. [4–27]. A similar combination of the effective confinement, approximated by the parabolic profile of the local refractive index, and the Kerr term is relevant as a model of optical waveguides [28–32]. Models of the same type find other physical realizations too, such as polariton condensates [33] and networks of Josephson oscillators [34].

The interplay of the self-attractive nonlinearity (self-focusing, in terms of optics) and trapping potential gives rise to localized modes, which may be considered as bright solitons confined by the external potential [35,36]. However, dynamics of solitons in expulsive potentials, such as an inverted HO (*anti-HO*), is also relevant in various physical settings [37–46]. In terms of optics, expulsive potentials represents antiwaveguiding setups, which are used in the design of photonic data-processing schemes [47–51]. It is worthy to mention that the interplay of the self-repulsive nonlinearity and a combination of spatially periodic (lattice) and HO or anti-HO potentials gives rise to gap solitons with a negative effective mass, which are expelled by the normal HO potential, and stay trapped under the action of the anti-HO one [52].

The objective of this work is to introduce a system of linearly coupled one- and two-dimensional (1D and 2D) "cores" (conduits for photonic or matter waves), with *opposite signs* of HO potentials acting in them, one confining and one

expulsive. In BEC, such a system can be built as a pair of parallel cigar- or pancake-shaped condensates coupled by tunneling of atoms, which may be enhanced by an additional optical link [53]. Then, the HO and anti-HO potentials in the cores can be induced by properly shaped red- and blue-detuned laser beams illuminating the cores (see, e.g., Ref. [54]). In optics, an effectively 1D coupler composed of planar waveguiding and antiwaveguiding cores can be fabricated in a straightforward way [55], although a 2D version of such an optical system is not a realistic one.

We consider these systems both in the linear regime and with inclusion of intra-core self-attractive or repulsive cubic nonlinearity. In fact, the linear version of the system is the most relevant one, as the existence of trapped states in the system with linearly-coupled components subject to the action of the confining and expulsive potentials is not obvious—in particular, because the straightforward definition of spectra does not directly apply to such a system. A *half-trapped* linearly coupled system, including the trapping HO potential in one component and no potential in the other, was considered recently [56], but, to the best of our knowledge, trapped-antitrapped systems were not addressed before.

It is obvious that, irrespective of the existence of confined states in the system with the antitrapping component, it also gives rise to a continuous family of delocalized states; therefore, the confined ones, if they exist, may be considered as a specific case of *bound states in the continuum* (BIC) [57–59], alias *embedded modes* [60]. Recently, applications of BIC of various types have drawn much interest in photonics [61–64].

The presentation is organized below as follows. The 1D and 2D systems are introduced in Sec. II. Then, Sec. III

reports exact analytical solutions of the *codimension-one* type (with one constraint imposed on the system's parameters), for both 1D and 2D systems in their linear form. These are ground-state (GS) and dipole-mode (DM) solutions in 1D, and 2D states with all integer values of vorticity, $S \geqslant 0$ ($S = 0$ represents the GS in 2D, while $S = 1$ is the 2D counterpart of the DM). The exact solutions play an important role, as they provide an *exact proof* of the existence of the bound state in the presence of the expulsive potential in one component. Generic, although approximate, analytical results and their numerical counterparts are produced, for the linear systems, in Sec. IV. The analytical results provide eigenvalues of the propagation constant, in terms of optics (or chemical potential, in BEC) for the GS and DM states in 1D, predicted by the variational (Rayleigh-Ritz) approximation. Another analytical finding is an asymptotic form, at $|x| \to \infty$ (or $r \to \infty$) of the 1D (or 2D) delocalized states. Effects of the nonlinearity are considered, in the numerical form, in Sec. V, which addresses stationary GS, DM, and 2D vortex modes in the nonlinear systems, and simulations of the evolution of inputs produced by exact eigenmodes of the linear system under the action of the nonlinearity. In the latter case, the system demonstrates the emergence of robust breathers for moderate nonlinearity, and chaotization when it is too strong. The vortex states in 2D are, as usual [65], unstable against spontaneous splitting under the action of self-attraction, and remain stable in the case of self-repulsion. The paper is concluded by Sec. VI.

II. THE ONE- AND TWO-DIMENSIONAL SYSTEMS

The 1D system is introduced, in the scaled form, as a pair of linearly coupled Schrödinger equations with the HO and anti-HO potentials in the first and second components. The equations are written in the notation adopted in optics, with propagation distance z and transverse coordinate x:

$$iu_z + \frac{1}{2}u_{xx} + \lambda v - \frac{1}{2}x^2 u + \sigma|u|^2 u = -\omega u, \quad (1)$$

$$iv_z + \frac{1}{2}v_{xx} + \lambda u + \frac{1}{2}\kappa x^2 v + \sigma|v|^2 v = 0. \quad (2)$$

Here the diffraction coefficients and strength of the HO trapping potential acting on the u component are normalized to be 1, λ is the coefficient of the linear coupling, which may be set to be positive, $\kappa > 0$ is the strength of the expulsive potential acting on v, and ω is a possible propagation-constant mismatch between the components. Finally, $\sigma = \pm 1$ or 0 represents the scaled nonlinearity coefficient, $\sigma = +1$ and -1 corresponding to the self-focusing and defocusing signs of the nonlinearity.

Stationary solutions to Eqs. (1) and (2) are looked for as

$$\{u, v\} = \{U(x), V(x)\} \exp(-i\mu z), \quad (3)$$

with real propagation constant $-\mu$ (in BEC, with z replaced by scaled time t, μ is the chemical potential), and real functions $U(x)$ and $V(x)$ satisfying equations

$$(\mu + \omega)U + \frac{1}{2}\frac{d^2 U}{dx^2} + \lambda V - \frac{1}{2}x^2 U + \sigma U^3 = 0, \quad (4)$$

$$\mu V + \frac{1}{2}\frac{d^2 V}{dx^2} + \lambda U + \frac{1}{2}\kappa x^2 V + \sigma V^3 = 0. \quad (5)$$

In fact, the nonlinearity plays a secondary role in the present context, the most important issue being the existence of trapped modes in the linear version of Eqs. (4) and (5), which corresponds to $\sigma = 0$. The main objective of the analysis presented below is finding spectra of eigenvalues μ for such modes.

The 2D version of the system, written in the polar coordinates (r, θ), is

$$iu_z + \frac{1}{2}\left(\frac{\partial^2}{\partial r^2} + \frac{1}{r}\frac{\partial}{\partial r} - \frac{1}{r^2}\frac{\partial^2}{\partial \theta^2}\right)u + \lambda v - \frac{1}{2}r^2 u + \sigma|u|^2 u$$
$$= -\omega u, \quad (6)$$

$$iv_z + \frac{1}{2}\left(\frac{\partial^2}{\partial r^2} + \frac{1}{r}\frac{\partial}{\partial r} - \frac{1}{r^2}\frac{\partial^2}{\partial \theta^2}\right)v + \lambda u + \frac{1}{2}\kappa r^2 v + \sigma|v|^2 v$$
$$= 0. \quad (7)$$

Stationary solutions to Eqs. (6) and (7) with integer vorticity S are looked for as

$$\{u, v\} = \exp(-i\mu z + iS\theta)\{U(r), V(r)\}, \quad (8)$$

where real functions U and V satisfy radial equations

$$(\mu + \omega)U + \frac{1}{2}\left(\frac{d^2}{dr^2} + \frac{1}{r}\frac{d}{dr} - \frac{S^2}{r^2}\right)U + \lambda V - \frac{1}{2}r^2 U + \sigma U^3$$
$$= 0, \quad (9)$$

$$\mu V + \frac{1}{2}\left(\frac{d^2}{dr^2} + \frac{1}{r}\frac{d}{dr} - \frac{S^2}{r^2}\right)V + \lambda U + \frac{1}{2}\kappa r^2 V + \sigma V^3 = 0. \quad (10)$$

Conserved quantities of the 1D system are the integral power (norm) and Hamiltonian,

$$P = \int_{-\infty}^{+\infty}[|u(x)|^2 + |v(x)|^2]dx \equiv P_u + P_v, \quad (11)$$

$$H = \int_{-\infty}^{+\infty}\left[\frac{1}{2}\left(|u_x|^2 + |v_x|^2 + |u|^2 - \kappa|v|^2\right) - \lambda(u^*v + uv^*)\right.$$
$$\left. + \frac{\sigma}{2}\left(|u|^4 + |v|^4\right)\right]dx. \quad (12)$$

The 2D system conserves obvious counterparts of integral quantities (11) and (12), and also the angular momentum,

$$M = -i\int_0^\infty r\,dr\int_0^{2\pi} d\theta\left(u^*\frac{\partial u}{\partial \theta} + v^*\frac{\partial v}{\partial \theta}\right), \quad (13)$$

where $*$ stands for the complex conjugate. Obviously, for eigenstates, Eqs. (8) and (13) have $M = SP$.

The evolution of the wave fields was simulated, in the framework of Eqs. (1), (2) and (6), (7), with the help of the MATLAB's ode15s program, which is a variable-step, variable-order solver based on the numerical differentiation formulas (NDFs) of orders up to 5. The spatial discretization was performed with a variable mesh size $\Delta x = \Delta y \lesssim 0.01$, and the propagation distance was discretized with a variable step size $\Delta z \lesssim 0.1$. Stationary Eqs. (4), (5) and (9), (10) were solved numerically by means of the collocation method, based on the Runge-Kutta algorithm, with the same values of Δx and Δy. All the equations were solved with the zero (Dirichlet) boundary conditions.

The size of Δx, Δy, and Δz, as well as the NDF order, were dynamically adjusted at each iteration step of the simulations, according to local error estimation, which had to satisfy the predefined tolerance. In the present work, the relative tolerance (pertaining to the local solution value) and the absolute tolerance were fixed as 10^{-3} and 10^{-6}, respectively. This choice made it possible to secure the stability of the numerical scheme. In particular, no visible change in the solutions was observed if the calculations were rerun with smaller values of Δx, Δy (up to 0.001), and Δz. In fact, some numerical results are plotted with values of Δx, Δy, and Δz somewhat larger than those which were used in the simulations, as very small values were not necessary for plotting.

III. EXACT SOLUTIONS FOR BOUND STATES IN THE LINEAR SYSTEM

A. The ground state

The linear version of the 1D stationary system, represented by Eqs. (4) and (5) with $\sigma = 0$, admits a *codimension-one* (non-generic) exact solution for the system's GS:

$$U(x) = \left(U_0 + U_2 x^2\right) \exp\left(-\frac{x^2}{2}\right), \qquad (14)$$

$$V(x) = V_0 \exp\left(-\frac{x^2}{2}\right), \qquad (15)$$

$$U_0 = \frac{1 + \kappa - 2\lambda^2}{4\lambda} V_0, \qquad (16)$$

$$U_2 = -\frac{1 + \kappa}{2\lambda} V_0, \qquad (17)$$

$$\mu_{\text{GS}} = \frac{1}{2}\left(\lambda^2 + \frac{1}{2}\right) - \frac{\kappa}{4}, \qquad (18)$$

where V_0 is an arbitrary amplitude. The codimension-one character of this solution is determined by the fact that it exists only if the following relation is imposed on parameters ω, κ, and λ:

$$\omega_{\text{GS}} = \frac{9}{4} - \frac{\lambda^2}{2} + \frac{\kappa}{4} \qquad (19)$$

(cf. Refs. [60] and [66], as concerns the definition of the codimensionality one). Note that, as it follows from Eqs. (14), (16), and (17), component $U(x)$ of the exact solution crosses zero at $x^2 = (1 + \kappa - 2\lambda^2)/[2(1 + \kappa)]$, under the condition of

$$\lambda^2 < (1/2)(1 + \kappa). \qquad (20)$$

Further, in the interval of

$$(1/2)(1 + \kappa) < \lambda^2 < (5/2)(1 + \kappa), \qquad (21)$$

$U(x)$ does not change its sign, but exhibits a local minimum at $x = 0$. An example of this feature is shown below, in the right panel of Fig. 1.

A "naive assumption" may be that the confined mode would be maintained by the linear coupling between U and V, in spite of the action of the expulsive potential upon the $V(x)$ component, if the naturally trapped one, $U(x)$, dominates in the system, i.e., if its integral power exceeds the power of V,
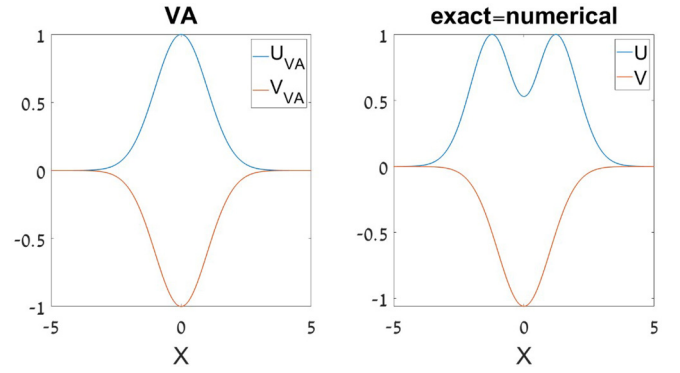
$$P_u/P_v > 1, \qquad (22)$$

FIG. 1. The right and left panels display, respectively, exact 1D GS (ground-state) solution of the linearized ($\sigma = 0$) version of Eqs. (4) and (5), and its VA-produced counterpart, at parameter values Eq. (52). Both the exact solution and VA yield, in this case, equal eigenvalues, $\mu_{\text{GS}} = \mu_{\text{GS}}^{(\text{VA})} = 1.5$. In these plots, the amplitude of the V component is set to be $V_0 = -1$. The top and bottom profiles depict components U and V, respectively.

see Eq. (11). Nevertheless, the confined mode may exist even if condition Eq. (22) does not hold. Indeed, for the exact solution Eqs. (14)–(17) the power ratio is

$$\left(\frac{P_u}{P_v}\right)_{\text{GS}} = \frac{\lambda^2}{4} + \frac{(1 + \kappa)^2}{8\lambda^2}. \qquad (23)$$

Straightforward analysis demonstrates that Eq. (23) always yields $P_u/P_v > 1$ if the strength of the expulsive potential is large enough, viz.,

$$\kappa > 2\sqrt{2} - 1 \approx 1.83, \qquad (24)$$

which agrees with the above-mentioned "naive" expectation. However, if condition Eq. (24) does not hold, then Eq. (23) gives $P_u/P_v < 1$ in the following interval of values of the coupling constant:

$$2 - \sqrt{4 - (1 + \kappa)^2/2} < \lambda^2 < 2 + \sqrt{4 - (1 + \kappa)^2/2}. \qquad (25)$$

B. The dipole mode (first excited state)

In addition to the spatially even GS solution, an exact odd one (DM), which represents the first excited state of the system, can be found too:

$$U(x) = (U_1 x + U_3 x^3) \exp\left(-\frac{x^2}{2}\right), \qquad (26)$$

$$V(x) = V_1 x \exp\left(-\frac{x^2}{2}\right), \qquad (27)$$

$$U_1 = \frac{3(1 + \kappa) - 2\lambda^2}{4\lambda} V_1, \qquad (28)$$

$$U_3 = -\frac{1 + \kappa}{2\lambda} V_1, \qquad (29)$$

$$\mu_{\text{DM}} = \frac{1}{2}\left(\lambda^2 + \frac{3}{2}\right) - \frac{3\kappa}{4}, \qquad (30)$$

where V_1 is an arbitrary amplitude. It is also a codimension-one solution, which exists if the following constraint is

imposed onto the parameters:

$$\omega_{\text{DM}} = \frac{11}{4} - \frac{\lambda^2}{2} + \frac{3\kappa}{4}, \tag{31}$$

cf. Eq. (19). Note that the special values of ω necessary for the existence of the GS and DM exact solutions, as given by Eqs. (19) and (31), respectively, cannot be equal for $\kappa > 0$. The wave function given by Eq. (26) crosses zero at finite values of x under condition

$$\lambda^2 < (3/2)(1 + \kappa), \tag{32}$$

cf. Eq. (20).

For the exact DM solution, the P_u/P_v ratio is given by

$$\left(\frac{P_u}{P_v}\right)_{\text{DM}} = \frac{\lambda^2}{4} + \frac{3(1 + \kappa)^2}{8\lambda^2}, \tag{33}$$

cf. Eq. (23). Accordingly, the U mode is always the dominant one ($P_u/P_v > 1$) in the case of

$$\kappa > 2\sqrt{2/3} - 1 \approx 0.63, \tag{34}$$

cf. Eq. (24). At smaller values of κ, there exist exact DM states with the dominance of the V mode, i.e., with $P_u/P_v < 1$.

C. 2D states

A particular exact solution of 2D stationary Eqs. (9) and (10) can also be found, for all integer values of vorticity S:

$$U(r) = \left(U_0^{(2D)} + U_2^{(2D)}r^2\right)r^S \exp\left(-\frac{r^2}{2}\right), \tag{35}$$

$$V(r) = V_0^{(2D)}r^S \exp\left(-\frac{r^2}{2}\right), \tag{36}$$

$$U_0^{(2D)} = \frac{(S + 1)(1 + \kappa) - \lambda^2}{2\lambda}V_0^{(2D)}, \tag{37}$$

$$U_2^{(2D)} = -\frac{1 + \kappa}{2\lambda}V_0^{(2D)}, \tag{38}$$

$$\mu_{2D} = \frac{1}{2}[\lambda^2 + (S + 1)(1 - \kappa)], \tag{39}$$

where $V_0^{(2D)}$ is an arbitrary amplitude. This solution too is of the codimension-one type, as it exists under the respective constraint:

$$\omega_{2D} = \frac{1}{2}[5 + S - \lambda^2 + (S + 1)\kappa]. \tag{40}$$

It is relevant to mention that the radial wave function Eq. (35) crosses zero at finite r under condition $\lambda^2 < (S + 1)(1 + \kappa)$, cf. similar condition Eqs. (20) and (32) in the 1D version of the system.

For the 2D GS solution with $S = 0$, the U component dominates, as per Eq. (22), at $\kappa > 1$, cf. Eqs. (24) and (34). In the opposite case, the V component is the dominant one in the interval of

$$2 - \sqrt{4 - (1 + \kappa)^2} < \lambda^2 < 2 + \sqrt{4 - (1 + \kappa)^2}, \tag{41}$$

cf. Eq. (25).

Finally, we note that all the exact solutions given by Eqs. (14)–(40) can be extended to the case of $\kappa < 0$, i.e., for the system in which both components are subject to the action of trapping potentials. In particular, codimension-one

exact solutions of the half-trapped system, corresponding to $\kappa = 0$, were recently found in Ref. [56]. In the latter case, all the exact solutions are of the BIC type.

IV. GENERIC SPECTRA OF THE BOUND STATES

A. The ground state of the 1D system

1. The variational approximation (VA)

The codimension-one exact solutions for the trapped modes with propagation constants given by Eqs. (18) and (30), obtained above for the 1D system, are valid only under constraints represented by Eq. (19) or Eq. (31), respectively. A possibility to predict generic trapped modes and the spectrum of their propagation constants is offered by the variational approximation (VA). Usually, it is applied to solitons and other modes in nonlinear systems [67], but its original form, known as the Rayleigh-Ritz approximation, was developed for finding spectra of linear systems, such as the Schrödinger equation in quantum mechanics [68,69]. In the present context, it is natural to apply it to the prediction of spectra of bound states in the system of Eqs. (4) and (5) in the linear limit, $\sigma = 0$.

In the framework of the VA, 1D wave functions of the GS may be approximated by the simplest ansatz

$$\left\{U_{\text{GS}}^{(\text{VA})}(x), V_{\text{GS}}^{(\text{VA})}(x)\right\} = \pi^{-1/4}\{\cos\eta, \sin\eta\} \exp\left(-\frac{x^2}{2}\right), \tag{42}$$

where η is a variational parameter, the Gaussian shape is suggested by the HO trapping potential in Eq. (4), and the ansatz is subject to the normalization condition,

$$\int_{-\infty}^{+\infty}\{[U(x)]^2 + [V(x)]^2\}dx = 1. \tag{43}$$

Next, one multiplies Eq. (4) with $\sigma = 0$ by $U(x)$, Eq. (5) by $V(x)$, integrates each one as $\int_{-\infty}^{+\infty} dx$, and takes the sum of the two. With regard to normalization condition Eq. (43), this procedure yields an expression for the eigenvalue sought for:

$$\mu = \int_{-\infty}^{+\infty} dx \left\{U(x)\left[-\omega U(x) - \frac{1}{2}\frac{d^2U}{dx^2} + \frac{1}{2}x^2U(x)\right] \right.$$
$$\left. + V(x)\left[-\frac{1}{2}\frac{d^2V}{dx^2} - \frac{\kappa}{2}x^2V(x)\right] - 2\lambda U(x)V(x)\right\}. \tag{44}$$

Formally, Eq. (44) gives an exact expression for μ, but written in terms of unknown wave functions $U(x)$ and $V(x)$. To obtain an actual result, we insert ansatz Eq. (42) and perform the integration, which yields the following approximate expression:

$$\mu_{\text{GS}}^{(\text{VA})} = \left(\frac{1}{2} - \omega\right)\cos^2\eta + \frac{1}{4}(1 - \kappa)\sin^2\eta - \lambda\sin(2\eta). \tag{45}$$

Now, the VA means minimization of this expression with respect to the free parameter, η, i.e., setting

$$\frac{d}{d\eta}(\mu^{(\text{VA})}) = 0. \tag{46}$$

The substitution of Eq. (45) in Eq. (46) produces the value of η sought for:

$$\tan(2\eta) = -\lambda/q_{\text{GS}}, \tag{47}$$

where

$$q_{\text{GS}} \equiv \frac{1}{2}\left[\frac{1}{4}(1+\kappa) - \omega\right]. \qquad (48)$$

Finally, the substitution of value Eq. (48) in the VA expression for μ, given by Eq. (45), leads to the following prediction for the eigenvalue:

$$\mu_{\text{GS}}^{\text{(VA)}} = \left(\frac{1}{2} - \omega - q_{\text{GS}}\right) + \sqrt{q_{\text{GS}}^2 + \lambda^2}. \qquad (49)$$

In particular, in the limit of $\kappa \to \infty$, i.e., in the limit of the very strong expulsive potential acting upon the V component, Eq. (49) yields

$$\mu_{\text{GS}}^{\text{(VA)}} \approx \frac{1}{2} - \omega + \frac{4\lambda^2}{\kappa}, \qquad (50)$$

which is close to the GS eigenvalue of the U component decoupled from V. Accordingly, in this limit Eqs. (42), (47), and (48) show that the relative amplitude of the V component in the bimodal bound state decreases as $V/U \approx \eta \approx -4\lambda/\kappa$. This result explains why the bound state can exist even under the action of the extremely strong expulsive potential acting upon the V component. However, the VA also admits GS solutions dominated by the V component, i.e., with $P_v > P_u$, see Eq. (22). The boundary of this situation corresponds to $\eta = \pi/4$ in ansatz (42), i.e., $q_{\text{GS}} = 0$, according to Eq. (47). Thus, it follows from Eq. (48) that the VA predicts the domination of the V component at $q_{\text{GS}} < 0$, i.e., at

$$\kappa < 4\omega - 1. \qquad (51)$$

2. Numerical results for the GS

Comparison of the VA-predicted profile of the GS, produced by Eqs. (42), (43), (47), and (48) at a generic point in the parameter space,

$$\kappa = 3, \lambda = 2, \omega = 1, \qquad (52)$$

which satisfies condition Eq. (19), with the exact profile, as given by Eqs. (14)–(17), is displayed in Fig. 1. Unlike the variational ansatz, the exact analytical solution features a local minimum at $x = 0$, as parameters Eq. (52) fall in interval Eq. (21). In spite of the discrepancy in the shape, in this case Eqs. (49) and (48) produce the VA eigenvalue $\mu_{\text{GS}}^{\text{(VA)}} = 1.5$, which *precisely* coincides with the exact eigenvalue given by Eq. (18).

The comprehensive results for the eigenvalue of the GS, as predicted by the VA and produced by the numerical solution of Eqs. (4) and (5) with $\sigma = 0$, are summarized, respectively, in the right and left panels of Fig. 2. It is seen that the trapped GS exists at all values of the strength of the expulsive potential (κ). Further, the VA produces quite accurate results, unless the strength λ of the linear coupling between the components U and V, upon which the HO and anti-HO potentials act, is too small. If λ is small, then it is not relevant to adopt the same functional form of both components in the ansatz; therefore, the variational ansatz Eq. (42) is inaccurate in that case.

The straight black line in the right bottom panel of Fig. 2 is the locus of points defined by Eq. (19), at which the exact solution is provided by Eqs. (14)–(18). Along this line, the eigenvalue of the numerically found GS solution is precisely
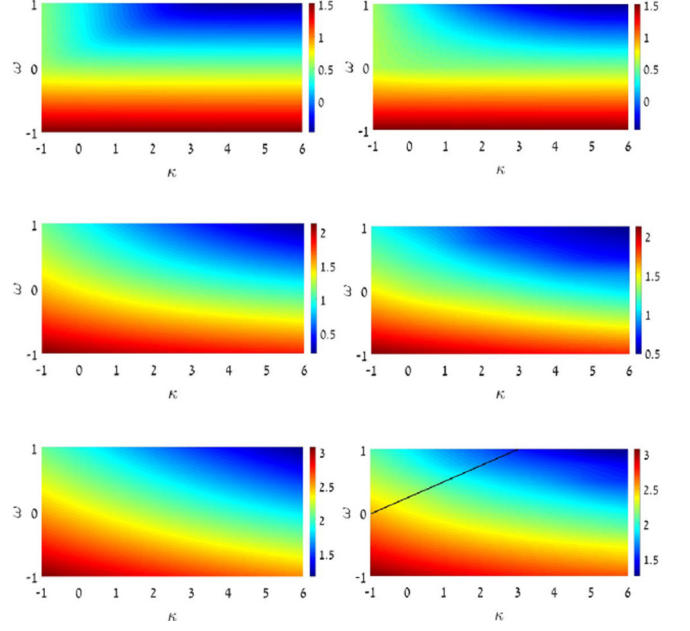

FIG. 2. Heatmaps (gray-scale maps, in the black-and-white rendition) of the GS eigenvalue in planes of strength κ of the expulsive potential and mismatch ω between the components, as produced by the numerical solution of the linearized Eqs. (4) and (5), and by the VA (the right and left panels, respectively). The top, middle, and bottom panels pertain, severally, to values of the inter-component coupling constant $\lambda = 0.1$, 1.0, and 2.0. The black line in the right bottom panel represents relation Eq. (19), at which the exact solution Eqs. (14)–(18) is available.

equal (up to the numerical accuracy) to the eigenvalue of the exact solution, as given by Eq. (18).

B. The dipole mode (DM) in the 1D system

1. The VA for the DM

The variational ansatz for the spatially odd DM solution is adopted as

$$\{U_{\text{DM}}^{\text{(VA)}}(x), V_{\text{DM}}^{\text{(VA)}}(x)\} = \sqrt{2}\pi^{-1/4}\{\cos\eta, \sin\eta\}x\exp\left(-\frac{x^2}{2}\right), \qquad (53)$$

cf. Eq. (42), which is also subject to normalization Eq. (43). Substituting this in Eq. (44) yields

$$\mu_{\text{DM}} = \left(\frac{3}{2} - \omega\right)\cos^2\eta + \frac{3}{4}(1-\kappa)\sin^2\eta - \lambda\sin(2\eta), \qquad (54)$$

cf. Eq. (45). Then, the variational Eq. (46), applied to Eq. (54), produces the result

$$\tan(2\eta) = -\lambda/q_{\text{DM}}, \qquad (55)$$

$$q_{\text{DM}} \equiv \frac{1}{2}\left[\frac{3}{4}(1+\kappa) - \omega\right], \qquad (56)$$

cf. Eqs. (47) and (48). The substitution of this in Eq. (54) leads to the following eigenvalue:

$$\mu_{\text{DM}}^{\text{(VA)}} = \frac{3}{2} - \omega - q_{\text{DM}} + \sqrt{q_{\text{DM}}^2 + \lambda^2}, \qquad (57)$$
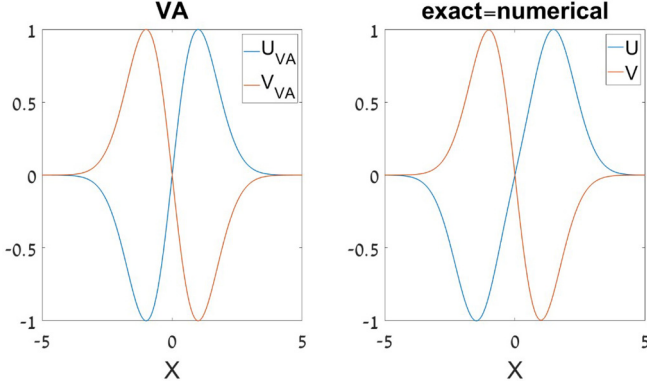
FIG. 3. The right and left panels display, respectively, the exact 1D DM (dipole-mode) solution of the linearized ($\sigma = 0$) version of Eqs. (4) and (5), and its variational counterpart, for parameters given by Eq. (59). Both the exact solution and VA give, in this case, equal eigenvalues, $\mu_{\mathrm{DM}} = \mu_{\mathrm{DM}}^{(\mathrm{VA})} = 2.5$. In these plots, the amplitude of the V component is $V_0 = -1$. In each panel, the right and left profiles depict components U and V, respectively.

cf. Eq. (49). In particular, in the limit of $\kappa \to \infty$, Eq. (57) gives

$$\mu_{\mathrm{DM}}^{(\mathrm{VA})} \approx \frac{3}{2} - \omega + \frac{4\lambda^2}{3\kappa}. \qquad (58)$$

Similar to Eq. (50), the latter result is close to the eigenvalue of the first excited state of the U component decoupled from V.

Also similar to what is considered above for the GS solution, the VA predicts that the V component is the dominant one in the DM ($P_v > P_u$) at $q_{\mathrm{DM}} < 0$, i.e., at $\kappa < (4/3)\omega - 1$, cf. Eq. (51).

2. Numerical results for the DM

At characteristic values of parameters,

$$\kappa = 1/3, \lambda = 2, \omega = 1, \qquad (59)$$

which satisfy condition Eq. (31), comparison of the variational profile of the DM, as produced by Eqs. (53), (43), (55), and (56), with the exact profile, as given by Eqs. (26)–(29) is displayed in Fig. 3. It is worthy to note that, in comparison with the GS (see Fig. 1), the VA profile for the DM is closer to its exact counterpart, although the two are not identical [ratios of amplitudes of the U and V components at parameter values Eq. (59) are 1 and 1.004, as given by the VA and exact solution, respectively]. Further, in this case Eqs. (57) and (56) produce the VA eigenvalue $\mu_{\mathrm{DM}}^{(\mathrm{VA})} = 2.5$, which precisely coincides with the exact eigenvalue given by Eq. (30).

Full results for the DM eigenvalue, as predicted by the VA, and as produced by the numerical solution of Eqs. (4) and (5) with $\sigma = 0$, are collected in the left and right panels of Fig. 4, respectively. As well as the GS, the DM trapped states exist at all values of the expulsive-potential's strength, κ. Also similar to what is observed in Fig. 2 for the GS, the VA predicts accurate results, unless the linear coupling λ is very small. The explanation of the latter point is the same as for the GS, *viz.*, ansatz Eq. (53) is inaccurate for small λ.
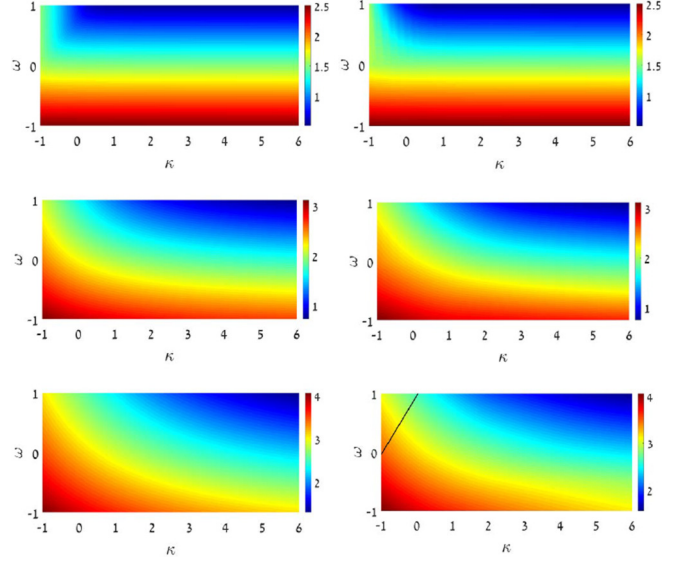

FIG. 4. Heatmaps (gray-scale maps, in the black-and-white rendition) of the DM eigenvalue in the (κ, ω) planes, as produced by the numerical solution of the linearized Eqs. (4) and (5), and by the VA (right and left panels, respectively). The top, middle, and bottom panels pertain to values of the coupling constant $\lambda = 0.1$, 1.0, and 2.0. The black line in the right bottom panel represents relation Eq. (31), at which the exact solution is given by Eqs. (26)–(30).

The straight black line in the right bottom panel of Fig. 4 is defined by Eq. (31), as the locus of points at which the exact DM solution exists. Along this line, the numerically found GS eigenvalue is precisely equal to its counterpart given by the exact solution, as per Eq. (18).

C. Numerical results for the 2D modes

It is commonly known that, due to the separability of the HO potential, the wave functions trapped in the 2D HO potential can be constructed as products of 1D eigenstates, and the 2D eigenvalue spectrum can be constructed, respectively, from its 1D counterpart. However, in the present system the factorization principle for the eigenstates is broken by linear-coupling terms. Therefore, it is necessary to compute eigenvalues of the 2D states numerically. It was thus found that, similar to the 1D case, the solutions for the bound states (at least, with vorticities $S = 0$ and 1) are produced by the numerical solution of the linear version of Eqs. (9) and (10) (with $\sigma = 0$) at all values of parameters κ, λ, and ω. A heatmap of the eigenvalues of the 2D states with $S = 0$ is displayed in Fig. 5.

The straight black line crossing the map in Fig. 5 is defined by Eq. (40). Along this line, the exact solution is given by Eqs. (35)–(38). The respective eigenvalue, given by Eq. (39), exactly coincides with its numerically found counterpart.

D. Delocalized states

The localized states considered above are dominated by the trapped component, U. The same system admits delocalized states, dominated by the antitrapped component, V. Exact solutions for delocalized states cannot be found even if the
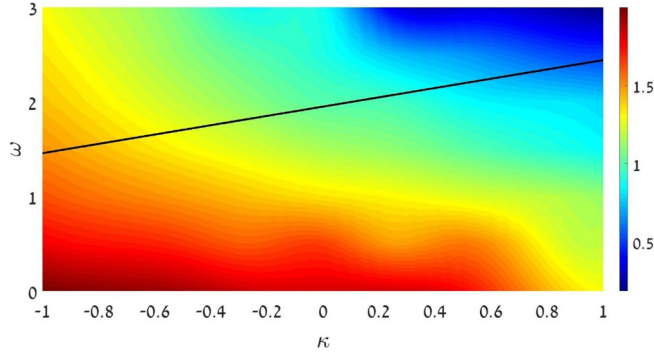
FIG. 5. The heatmap (gray-scale map, in the black-and-white rendition) of the eigenvalue of the 2D trapped state with $S = 0$ (zero vorticity) in the (κ, ω) plane at $\lambda = 1$, as produced by the numerical solution of the linearized Eqs. (9) and (10). The black line represents the relation given by Eq. (40), at which the exact 2D solution is given by Eqs. (35)–(39).

system is taken in the linearized form, with $\sigma = 0$, but it is possible to construct an asymptotic form of such states at $|x| \to \infty$. The consideration of Eqs. (4) and (5) yields

$$V_{\text{deloc}}(x) \underset{|x| \to \infty}{\approx} V_0 |x|^{-1/2} \cos\left(\frac{\sqrt{\kappa}}{2} x^2 + \frac{\mu}{\sqrt{\kappa}} \ln(|x|) \right), \quad (60)$$

$$U_{\text{deloc}}(x) \underset{|x| \to \infty}{\approx} V_0 \frac{2\lambda}{1 + \kappa} |x|^{-5/2} \cos\left(\frac{\sqrt{\kappa}}{2} x^2 + \frac{\mu}{\sqrt{\kappa}} \ln(|x|) \right), \quad (61)$$

where V_0 is an arbitrary constant. Obviously, the total power of the V component of this solution, defined as per Eq. (11), diverges as $\int dx/|x|$ at $|x| \to \infty$; therefore, such states are categorized as delocalized ones. The principal difference of the delocalized states from the trapped ones, in addition to the divergence of the norm, is that they form a *continuous spectrum*, with the delocalized solutions existing at all values of μ, as seen from Eqs. (60) and (61), while the localized
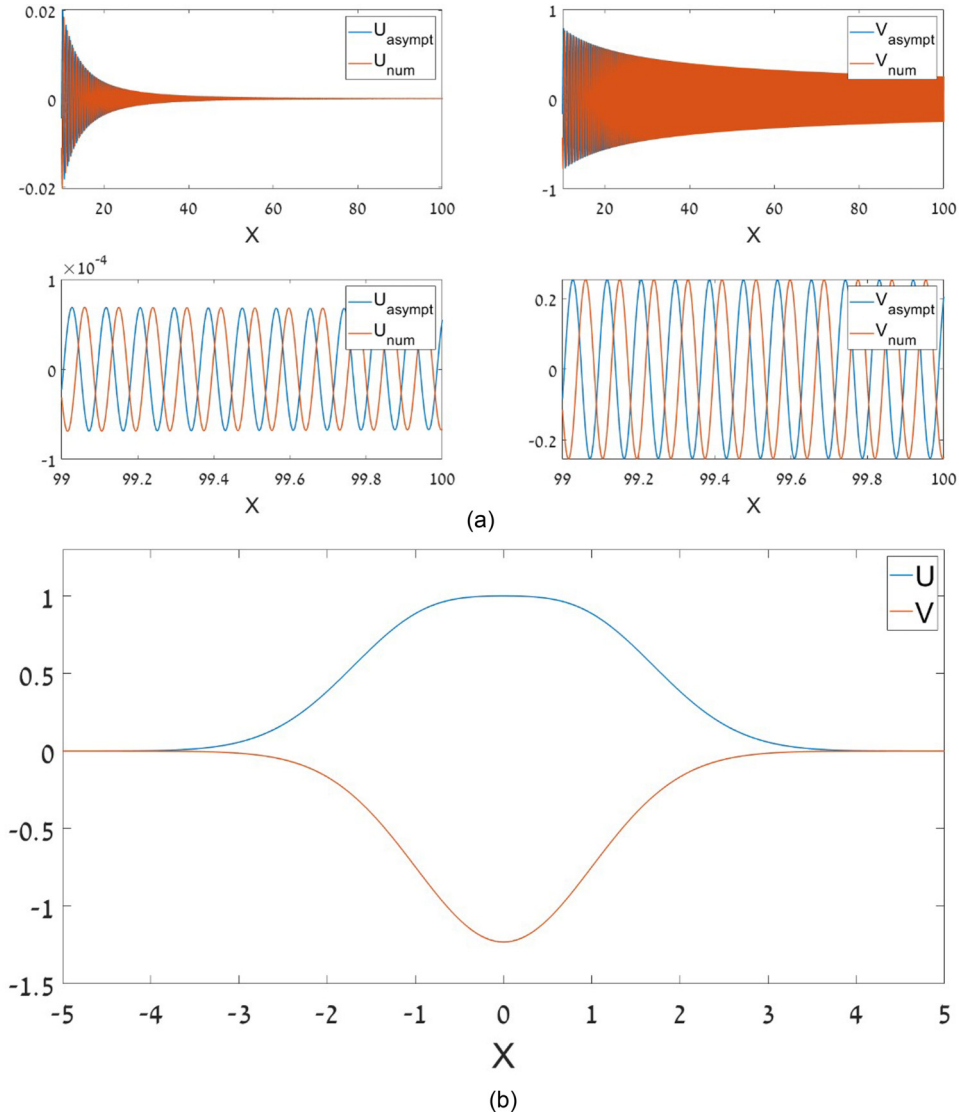

(a)

(b)

FIG. 6. (a) Numerically found shapes of the two components of a delocalized mode with parameters given by Eq. (62), and their counterparts predicted by the asymptotic expressions given by Eqs. (60) and (61). (b) The exact GS solution given by Eqs. (14)–(18) for the same parameters, with the top and bottom profiles depicting $U(x)$ and $V(x)$, respectively.

states form the *discrete spectrum*: GS, DM, etc. Furthermore, the trapped states may be considered as BIC ones, as discrete values of μ corresponding to them are embedded into the continuous spectrum of the delocalized states.

A typical example of the delocalized states is displayed in Fig. 6(a), along with the analytical asymptotic form, predicted by Eqs. (60) and (61), for parameters

$$\kappa = 0.5, \; \lambda = 2, \; \omega = 0.375, \; \mu = 2.125. \quad (62)$$

These values are chosen because they satisfy Eq. (19), hence the exact GS solution, given by Eqs. (14)–(17), is available in this case, with the corresponding propagation constant $\mu = 2.125$ given by Eq. (18). This GS solution is plotted in Fig. 6(b). Thus, the existence of the delocalized state with exactly the same value of μ directly corroborates that the localized states may be considered as ones of the BIC type. Further, it is seen that the overall shape of the analytical prediction of the delocalized state is quite accurate, some discrepancy being represented by a phase shift of the oscillating carrier waves. In particular, the numerical solution corroborates the fact that the dominant role is played by the V component.

Similarly, in the 2D case the asymptotic form of solutions to Eqs. (9) and (10) for delocalized states is

$$V_{\text{deloc}}^{(2D)}(r) \underset{r \to \infty}{\approx} V_0 r^{-1} \cos\left(\frac{\sqrt{\kappa}}{2} r^2 + \frac{\mu}{\sqrt{\kappa}} \ln r\right), \quad (63)$$

$$U_{\text{deloc}}^{(2D)}(r) \underset{r \to \infty}{\approx} V_0 \frac{2\lambda}{1+\kappa} r^{-3} \cos\left(\frac{\sqrt{\kappa}}{2} r^2 + \frac{\mu}{\sqrt{\kappa}} \ln r\right). \quad (64)$$

As well as in the 1D case, the 2D delocalized states form a continuous spectrum, existing at all values of μ, and their total power (norm),

$$P_{2D} = 2\pi \int_0^\infty \left[U^2(r) + V^2(r)\right] r \, dr, \quad (65)$$

diverges at $r \to \infty$ as $\int dr/r$.

V. BOUND STATES AND THEIR DYNAMICS IN NONLINEAR SYSTEMS

A. Ground states and dipole modes in 1D

As mentioned above, the results obtained for the linear systems are most essential for the analysis of the concept of trapped states in the expulsive potential, maintained by the linear coupling to the component confined by the trapping potential. Nevertheless, it is also interesting to consider the role of the nonlinearity in Eqs. (1), (2) and (4), (5).

First, taking into regard the nonlinear terms with $\sigma = +1$ or -1 (self-attraction or repulsion) in Eqs. (4) and (5) leads to moderate deformation of the 1D GS solution, as shown in Fig. 7 for the set of parameters

$$\kappa = 1, \lambda = 5, \omega = -10. \quad (66)$$

These values satisfy condition Eq. (19), hence the solution with $\sigma = 0$ is given in the exact form by Eqs. (14)–(17), with the respective eigenvalue $\mu = 12.5$ given by Eq. (18). Naturally, the self-compression ($\sigma = +1$) and repulsion ($\sigma = -1$) tend to make the trapped states slightly narrower or broader, respectively. Direct simulations of the perturbed evolution in
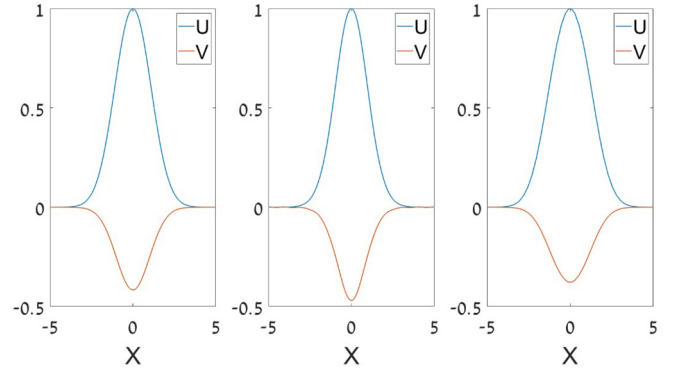

FIG. 7. The left, central, and right panels show, respectively, the exact 1D GS solution at parameter values Eq. (66) and its counterparts produced by the numerical solution of Eqs. (4) and (5) for $\sigma = +1$ and -1. The eigenvalues of the three solutions are $\mu = 12.5$, 11.9735, and 13.1925. All the solutions are produced with the amplitude of the U component $U(x=0) = 1$. The top and bottom profiles depict components $U(x)$ and $V(x)$, respectively.

the framework of Eqs. (1) and (2) demonstrate that that the nonlinearly deformed solutions remain stable (not shown here in detail).

The nonlinear shift of the eigenvalues can be roughly estimated, in the Thomas-Fermi approximation, by combining Eqs. (4) and (5) at the central point and neglecting the second-derivative terms,

$$\delta\mu \simeq -\sigma\left(U_0^4 + V_0^4\right)/\left(U_0^2 + V_0^2\right) \simeq \mp 0.85, \quad (67)$$

for $\sigma = \pm 1$. This estimate is consistent with the numerically found shift $|\delta\mu| \simeq 0.7$ for the nonlinear solutions displayed in Fig. 7. Furthermore, the sign of $\delta\mu$ in Eq. (67) implies that the GS family in the nonlinear system with $\sigma = +1$ satisfies the Vakhitov-Kolokolov (VK) criterion, $d\mu/dP < 0$ [recall P is the total power defined as per Eq. (11)], which is the well-known condition necessary for the stability of GS modes in systems of the nonlinear-Schrödinger type with self-attraction [70–72]. For $\sigma = -1$, Eq. (67) implies $d\mu/dP > 0$, which means that, in the case of the self-repulsion, the GS solutions satisfy the *anti-VK* criterion, which is a necessary stability condition for ground states in the case of self-repulsion [73].

The nonlinearity produces a still smaller change of the shape and eigenvalue of the trapped DM. As an example, Fig. 8 displays it for parameters

$$\kappa = 2.5, \lambda = 10, \omega = -45.375, \quad (68)$$

which satisfy condition Eq. (40), hence the linear DM solution (shown in the left panel of Fig. 8) is available in the exact form, according to Eqs. (26)–(29), with the respective eigenvalue $\mu = 48.875$ given by Eq. (30). Note that the sign of the nonlinearity-induced shift of the eigenvalue is the same as in Eq. (67).

To explore robustness of bound states in the present setting, it is also relevant to simulate evolution of an input, taken as an analytical or numerical eigenstate of the linear system, in the framework of the full nonlinear system of Eqs. (1) and (2). The conclusion is that, if the nonlinearity is moderately strong (in other words, if the input's amplitude is not too large), the linear eigenstate spontaneously transforms into a
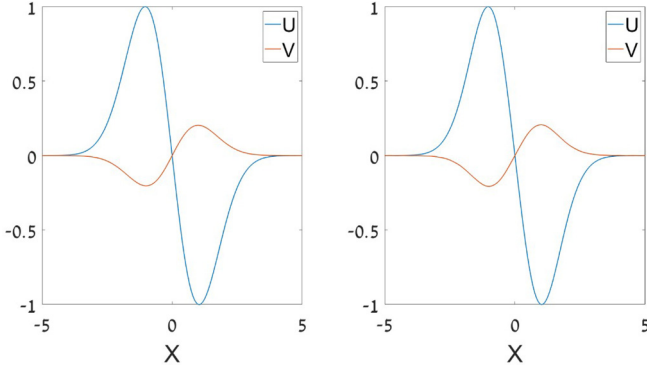
FIG. 8. The left and right panels show, respectively, the exact 1D DM solution at parameter values Eq. (68) and its counterpart produced by the numerical solution of Eqs. (4) and (5) for $\sigma = +1$. The eigenvalues of the linear and nonlinear solutions are, respectively, $\mu = 48.875$ and 48.3634. The solutions are produced with the amplitude of the U component $U_{\max} = 1$. The large- and small-amplitude profiles depict components U and V, respectively. The solution for $\sigma = -1$ (not shown here) is very close to these ones.

robustly oscillating breather. The respective examples for the GS and DM are presented, severally, in Fig. 9 for

$$\kappa = 1, \lambda = 6, \omega = -15.5, \tag{69}$$

and in Fig. 10 for

$$\kappa = 0.5, \lambda = 5, \omega = -9.375. \tag{70}$$

The regular oscillations carry over into chaotic dynamics when the amplitude exceeds a certain critical value. For instance, the GS input, given by Eqs. (14)–(17) with parameters from Eq. (69) and amplitude V_0, evolves into a chaotic state at $|V_0| > (|V_0|)_{\mathrm{crit}} \simeq 0.75$ for $\sigma = +1$, and $|V_0| > (|V_0|)_{\mathrm{crit}} \simeq 1$ for $\sigma = -1$ (these values correspond to amplitudes $U_0 \simeq 2.3$ and $U_0 \simeq 3$, respectively). It is natural that the chaotic behavior commences later in the case of the self-defocusing nonlinearity. Similarly, in the case of the DM input given by Eqs. (14)–(17) with parameters from Eq. (70), the chaotization threshold is found at $(|V_0|)_{\mathrm{crit}} \simeq 2$ [which corresponds to $(|U(x)|)_{\max} \simeq 3$] for both signs of the nonlinearity, $\sigma = \pm 1$.
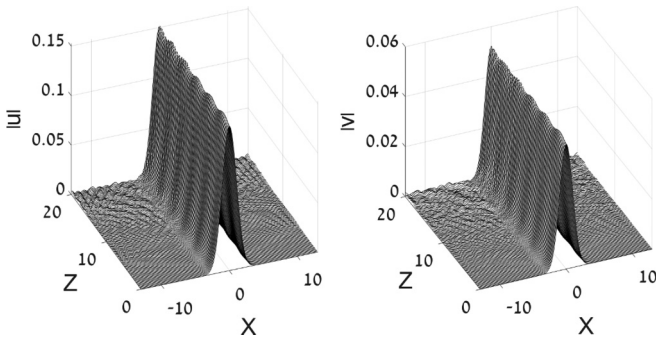

FIG. 9. Robust oscillations produced by simulations of Eqs. (1) and (2) with parameters from Eq. (69) and $\sigma = +1$, and the input given by the linear GS eigenmode from Eqs. (14)–(17) with amplitude $V_0 = -0.05$ (it corresponds to $U_0 = 0.146$).
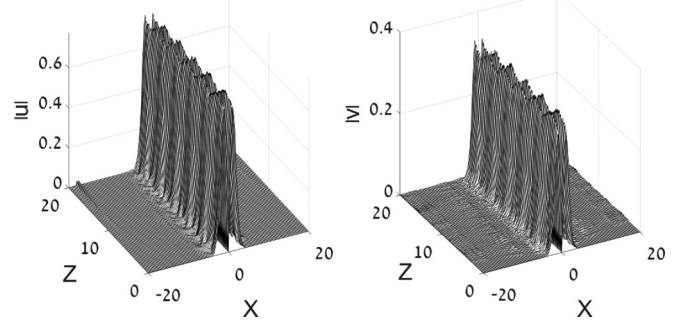

FIG. 10. The same as in Fig. 9, but for parameters from Eq. (70) and the input given by the linear DM eigenmode from Eqs. (26)–(29) with amplitude $V_1 = -0.5$ (it corresponds to amplitude $U_{\max} = 0.716$).

An example of the spontaneously established chaos is displayed in Fig. 11. It demonstrates that the chaotization effectively destroys the coupling between the two components; as a result, the v field expands over the entire integration domain, under the action of the anti-OH potential, while the u field stays confined by the HO potential acting upon it.

B. The ground and vortical states in 2D

As shown in Figs. (12) and (13), the moderate nonlinearity included in 2D stationary Eqs. (9) and (10) leads to weak deformation of the radial profile of the GS ($S = 0$) and vortices, and a very small shift of their propagation constants. In particular, Fig. (12) displays the GS radial profiles for parameters

$$\kappa = 1, \ \lambda = 5, \ \omega = -12, \tag{71}$$

which satisfy condition Eq. (40) with $S = 0$, thus supplying the exact solution for $\sigma = 0$, as given by Eqs. (35)–(39). Note that the difference between the eigenvalues of the nonlinear and linear solutions in Fig. (12), $\delta\mu \approx -0.4$, demonstrates that the 2D GS solutions also satisfy the VK criterion in the case of the self-focusing nonlinearity. In agreement with this fact, direct simulations corroborate the stability of these solutions. Similarly, in the case of self-defocusing, $\sigma = -1$, the nonlinear deformation and eigenvalue shift are very small too, and the respective GS solutions satisfy the anti-VK criterion. Their stability was also verified in direct simulations (not shown here).
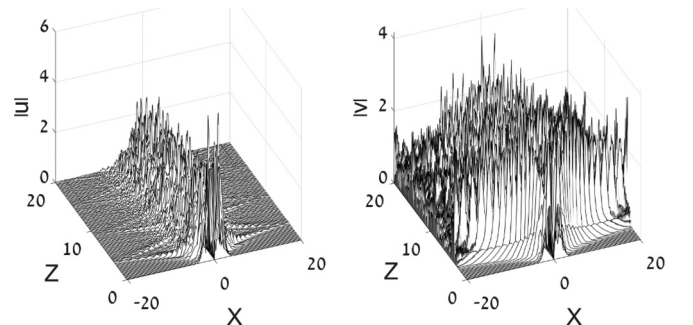

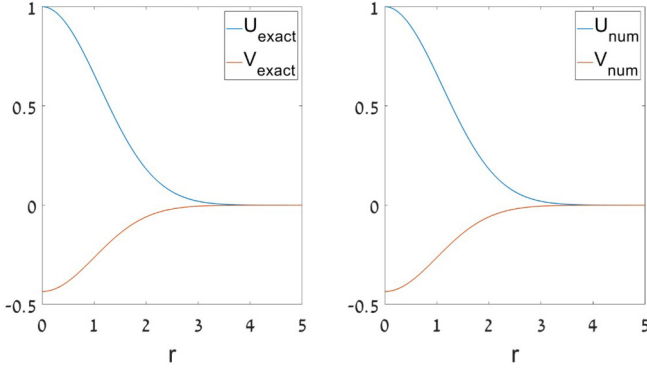FIG. 11. The same as in Fig. 10, but for amplitude $V_1 = 2.5$ of the DM input.

FIG. 12. The left and right panels display, respectively, the radial profile of the exact solution given by Eqs. (35)–(39) for the 2D GS ($S = 0$) in the linear system ($\sigma = 0$), with parameters from Eq. (71), $\mu = 12.5$, and its counterpart produced by the numerical solution of Eqs. (9) and (10) with $\sigma = +1$, the respective eigenvalue being $\mu = 12.10$. The amplitude of the U component of both solutions is set to be $U_0 = 1$. The top and bottom profiles depict components $U(r)$ and $V(r)$, respectively.

Typical examples of the exact linear solution for the vortex mode with $S = 1$ and its nonlinear counterpart, produced by the numerical solution of Eqs. (9) and (10) with $\sigma = +1$, are presented in Fig. 13. The parameters are chosen as

$$\kappa = 0.5, \ \lambda = 10, \ \omega = -46.5, \quad (72)$$

satisfying the condition given by Eq. (40) In this case too, the nonlinearity-induced deformation of the radial profile and eigenvalue shift, $\delta\mu$, are relatively small, and the sign of $\delta\mu$ is the same as given by Eq. (67).

While direct simulations demonstrate that the 2D states with $S = 0$ are completely stable under the action of the nonlinearity of either sign (not shown here in detail), a well-known problem for localized vortex states in systems with the self-attractive nonlinearity is their instability against spontaneous splitting [12,74–76] (see also a review in Ref. [65]). For the present system, we addressed this issue by means of direct simulations of the evolution of 2D states with $S = 1$
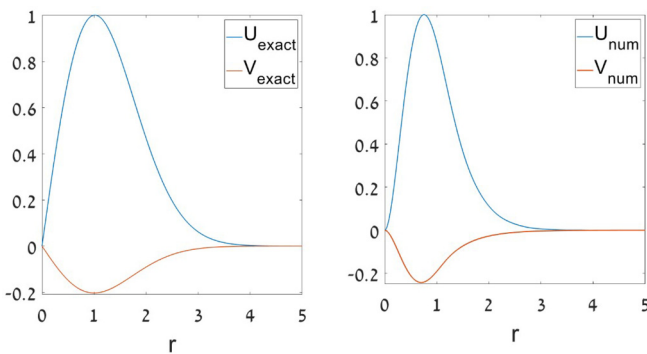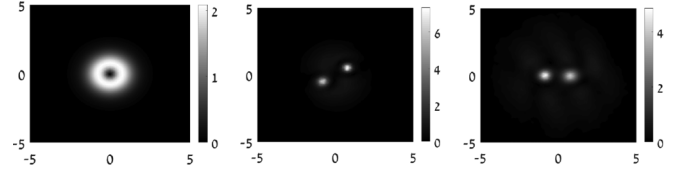

FIG. 14. Spontaneous splitting of the vortex state with $S = 1$, produced by simulations of Eqs. (6) and (7) with parameters from Eq. (72). The input was provided by the numerical solution of the stationary equations which is plotted in the right panel of Fig. 13. The three plots display distributions of density $|u(x, y; z)|^2$ at values of the propagation distance $z = 0$ (input), 3.8, and 6.2.

in the framework of Eqs. (6) and (7). While we did not aim to explore the entire family of the solutions, the result is that the vortices are indeed unstable against splitting into a pair of fragments in the self-focusing system (with $\sigma = +1$), which is a generic outcome of the instability development known in other systems [65]. A typical example of the splitting is displayed in Fig. 14. The rotation of the pair, observed in the figure, provides conservation of the angular momentum defined by Eq. (13).

However, direct simulations demonstrate that vortices with $S = 1$ are stable in the self-defocusing system ($\sigma = -1$). An example of the radial profile of the vortex in this case is plotted (along with its counterpart provided by the exact solution of the linear system) in Fig. 15, for parameters

$$\kappa = 1, \ \lambda = 7, \ \omega = -20.5, \quad (73)$$

that satisfy Eq. (40). In this case, the nonlinear deformation and shift of the propagation constant are quite small too. Stability of vortices under the action of the self-repulsion is corroborated by direct simulations, see Fig. 16.

VI. CONCLUSION

The objective of this work is to demonstrate the existence of stable bound states in the 1D and 2D linearly-coupled two-component systems, with the trapping HO (harmonic-oscillator) and expulsive anti-HO potentials acting upon the
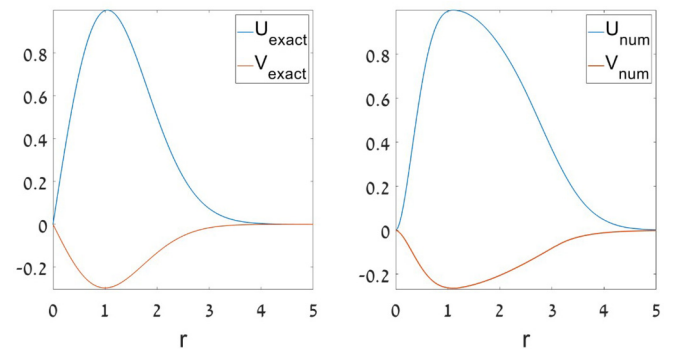

FIG. 13. The same as in Fig. 12, but for vortex states with $S = 1$ and parameters from Eq. (72). The eigenvalues are $\mu = 50.5$ and 48.5213 for the linear and nonlinear solutions, respectively. The amplitude of the U component of both solutions is set to be $[U(r)]_{\max} = 1$. The top and bottom profiles depict components $U(r)$ and $V(r)$, respectively.

FIG. 15. The same as in Fig. 13, but for vortex states with $\sigma = -1$ and parameters from Eq. (73). The eigenvalues are $\mu = 24.5$ and 27.011 for the linear and nonlinear solutions, respectively. The amplitude of the U component of both solutions is set to be $[U(r)]_{\max} = 1$. The top and bottom profiles depict components $U(r)$ and $V(r)$, respectively.
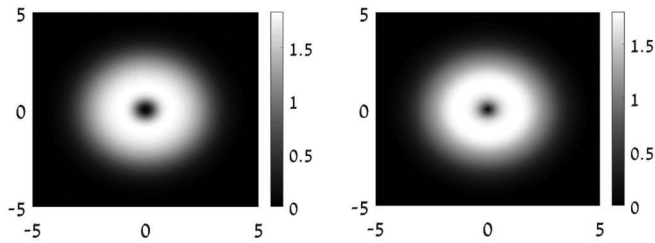
FIG. 16. Stability of the vortex state with $S = 1$, whose stationary profile is shown in Fig. 15(b), corroborated by simulations of Eqs. (6) and (7) with parameters from Eq. (73) and $\sigma = -1$. Left and right plots display, respectively, distributions of density $|u(x, y; z)|^2$ at $z = 0$ and 10.

components. The systems can be realized in optics and BEC. Exact analytical solutions, which are subject to the codimension-one constraints, and generic solutions, produced by the VA (variational approximation) and obtained in the numerical form, demonstrate that the linear systems support the GS (ground state) and DM (dipole mode, i.e., the first excited state), as well as 2D vortex states with all integer values of the vorticity, at all values of the system's parameters. Thus, the linear coupling to the trapped component makes it possible to maintain robust localized states in the component subject to the action of the expulsive potential. In most cases, the trapped component is the dominant one, in terms of the integral power (norm). Nevertheless, there is a parameter region in which the antitrapped component has a larger power. The confined modes supported by this system may be considered as BIC (bound states in continuum), as they coexist with delocalized states which form the continuous spectrum. The asymptotic form of the delocalized solutions is obtained analytically. The inclusion of the self-attractive or repulsive nonlinearity slightly deforms the 1D states, as well as the 2D GS, which remain stable solutions. However, the self-attraction leads to the splitting instability of vortices, while they remain stable under the action of self-repulsion.

The work may be extended by considering higher-order eigenstates in 1D, and performing a more systematic analysis of 2D vortex states. It may also be interesting to consider coherent motion of self-trapped states in the 1D and 2D systems, cf. Refs. [77] and [10].

[1] C. J. Pethick and H. Smith, *Bose-Einstein Condensation in Dilute Gases* (Cambridge University Press, Cambridge, UK, 2002).

[2] L. P. Pitaevskii and S. Stringari, *Bose-Einstein Condensation* (Oxford University Press, Oxford, UK, 2003).

[3] P. G. Kevrekidis, D. J. Frantzeskakis, and R. Carretero-González, *Emergent Nonlinear Phenomena in Bose-Einstein Condensates: Theory and Experiment* (Springer, Heidelberg, 2008).

[4] S. Grossmann and M. Holthaus, On Bose-Einstein condensation in harmonic traps, Phys. Lett. A **208**, 188 (1995).

[5] Y. Castin and R. Dum, Bose-Einstein Condensates in Time-Dependent Traps, Phys. Rev. Lett. **77**, 5315 (1996).

[6] A. L. Fetter and D. L. Feder, Beyond the Thomas-Fermi approximation for a trapped condensed Bose-Einstein gas, Phys. Rev. A **58**, 3185 (1998).

[7] H. Pu, C. K. Law, J. H. Eberly, and N. P. Bigelow, Coherent disintegration and stability of vortices in trapped Bose condensates, Phys. Rev. A **59**, 1533 (1999).

[8] B. I. Schneider and D. L. Feder, Numerical approach to the ground and excited states of a Bose-Einstein condensed gas confined in a completely anisotropic trap, Phys. Rev. A **59**, 2232 (1999).

[9] S. K. Adhikari, Numerical solution of the two-dimensional Gross-Pitaevskii equation for trapped interacting atoms, Phys. Lett. A **265**, 91 (2000).

[10] T. Busch and J. R. Anglin, Motion of Dark Solitons in Trapped Bose-Einstein Condensates, Phys. Rev. Lett. **84**, 2298 (2000).

[11] Y. S. Kivshar, T. J. Alexander, and S. K. Turitsyn, Nonlinear modes of a macroscopic quantum oscillator, Phys. Lett. A **278**, 225 (2001).

[12] T. J. Alexander and L. Bergé, Ground states and vortices of matter-wave condensates and optical guided waves, Phys. Rev. E **65**, 026611 (2002).

[13] G. Huang, J. Szeftel, and S. Zhu, Dynamics of dark solitons in quasi-one-dimensional Bose-Einstein condensates, Phys. Rev. A **65**, 053605 (2002).

[14] N. G. Parker, N. P. Proukakis, M. Leadbeater, and C. S. Adams, Soliton-Sound Interactions in Quasi-One-Dimensional Bose-Einstein Condensates, Phys. Rev. Lett. **90**, 220401 (2003).

[15] D. E. Pelinovsky, D. J. Frantzeskakis, and P. G. Kevrekidis, Oscillations of dark solitons in trapped Bose-Einstein condensates, Phys. Rev. E **72**, 016615 (2005).

[16] V. A. Brazhnyi and V. V. Konotop, Stable and unstable vector dark solitons of coupled nonlinear Schrödinger equations: Application to two-component Bose-Einstein condensates, Phys. Rev. E **72**, 026616 (2005).

[17] M. I. Merhasin, B. A. Malomed, and R. Driben, Transition to miscibility in a binary Bose-Einstein condensate induced by linear coupling, J. Phys. B **38**, 877 (2005).

[18] D. Mihalache, D. Mazilu, B. A. Malomed, and F. Lederer, Vortex stability in nearly-two-dimensional Bose-Einstein condensates with attraction, Phys. Rev. A **73**, 043615 (2006).

[19] H. E. Nistazakis, D. J. Frantzeskakis, P. G. Kevrekidis, B. A. Malomed, and R. Carretero-Gonzalez, Bright-dark soliton complexes in spinor Bose-Einstein condensates, Phys. Rev. A **77**, 033612 (2008).

[20] N. G. Parker, N. G. Proukakis, and C. S. Adams, Dark soliton decay due to trap anharmonicity in atomic Bose-Einstein condensates, Phys. Rev. A **81**, 033606 (2010).

[21] S. Alama, L. Bronsard, A. Contreras, and D. E. Pelinovsky, Domains walls in the coupled Gross-Pitaevskii equations, Arch. Ration. Mech. Anal. **215**, 579 (2015).

[22] Z. Chen, Y. Li, B. A. Malomed, and L. Salasnich, Spontaneous symmetry breaking of fundamental states, vortices, and dipoles in two and one-dimensional linearly coupled traps with cubic self-attraction, Phys. Rev. A **96**, 033621 (2017).

[23] T. Bland, N. G. Parker, N. P. Proukakis, and B. A. Malomed, Probing quasi-integrability of the Gross-Pitaevskii equation in a harmonic-oscillator potential, J. Phys. B: At. Mol. Opt. Phys. **51**, 205303 (2018).

[24] H. Sakaguchi and B. A. Malomed, Symmetry breaking in a two-component system with repulsive interactions and linear coupling, Commun. Nonlin. Sci. Numer. Simulat. **92**, 105496 (2021).

[25] P. Bizoń, F. Ficek, D. E. Pelinovsky, and S. Sobieszek, Ground state in the energy super-critical Gross-Pitaevskii equation with a harmonic potential, Nonlin. Anal. **210**, 112358 (2021).

[26] A. Biasi, O. Evnin, and B. A. Malomed, Fermi-Pasta-Ulam phenomena and persistent breathers in the harmonic trap, Phys. Rev. E **104**, 034210 (2021).

[27] B. A. Malomed, New findings for the old problem: Exact solutions for domain walls in coupled real Ginzburg-Landau equations, Phys. Lett. A **422**, 127802 (2022).

[28] S. Raghavan and G. P. Agrawal, Spatiotemporal solitons in inhomogeneous nonlinear media, Opt. Commun. **180**, 377 (2000).

[29] D. A. Zezyulin, G. L. Alfimov, and V. V. Konotop, Nonlinear modes in a complex parabolic potential, Phys. Rev. A **81**, 013606 (2010).

[30] E. G. Charalampidis, P. G. Kevrekidis, D. J. Frantzeskakis, and B. A. Malomed, Dark-bright solitons in coupled NLS equations with unequal dispersion coefficients, Phys. Rev. E **91**, 012924 (2015).

[31] Y. Zhang, X. Liu, M. R. Belić, W. Zhong, Y. Zhang, and M. Xiao, Propagation Dynamics of a Light Beam in a Fractional Schrödinger Equation, Phys. Rev. Lett. **115**, 180403 (2015).

[32] T. Mayteevarunyoo, B. A. Malomed, and D. V. Skryabin, One- and two-dimensional modes in the complex Ginzburg-Landau equation with a trapping potential, Opt. Express **26**, 8849 (2018).

[33] R. Balili, V. Hartwell, D. Snoke, L. Pfeiffer, and K. West, Bose-Einstein condensation of microcavity polaritons in a trap, Science **316**, 1007 (2007).

[34] M. Leib, F. Deppe, A. Marx, R. Gross, and M. J. Hartmann, Networks of nonlinear superconducting transmission line resonators, New J. Phys. **14**, 075024 (2012).

[35] Y. S. Kivshar and G. P. Agrawal, *Optical Solitons: From Fibers to Photonic Crystals* (Academic Press, San Diego, CA, 2003).

[36] T. Dauxois and M. Peyrard, *Physics of Solitons* (Cambridge University Press, Cambridge, UK, 2006).

[37] L. D. Carr and Y. Castin, Dynamics of a matter-wave bright soliton in an expulsive potential, Phys. Rev. A **66**, 063602 (2002).

[38] L. Salasnich, Dynamics of a Bose-Einstein-condensate bright soliton in an expulsive potential, Phys. Rev. A **70**, 053617 (2004).

[39] Z. X. Liang, Z. D. Zhang, and W. M. Liu, Dynamics of a Bright Soliton in Bose-Einstein Condensates with Time-Dependent Atomic Scattering Length in an Expulsive Parabolic Potential, Phys. Rev. Lett. **94**, 050402 (2005).

[40] W. B. Cardoso, A. T. Avelar, and D. Bazeia, Bright and dark solitons in a periodically attractive and expulsive potential with nonlinearities modulated in space and time, Nonlin. Analysis Real World Appl. **11**, 4269 (2010).

[41] S. Rajendran, P. Muruganandam, and M. Lakshmanan, Bright and dark solitons in a quasi-1D Bose-Einstein condensates modelled by 1D Gross-Pitaevskii equation with time-dependent parameters, Physica D **239**, 366 (2010).

[42] N. H. Xuan and M. Zuo, Matter-wave solitons in two-component Bose-Einstein condensates with tunable interactions and time varying potential, Commun. Theor. Phys. **56**, 1035 (2011).

[43] S. Rajendran, M. Lakshmanan, and P. Muruganandam, Matter wave switching in Bose-Einstein condensates via intensity redistribution soliton interactions, J. Math. Phys. **52**, 023515 (2011).

[44] A. del Campo and M. G. Boshier, Shortcuts to adiabaticity in a time-dependent box, Sci. Rep. **2**, 648 (2012).

[45] R. Radha, P. S. Vinayagam, J. B. Sudharsan, and B. A. Malomed, Persistent bright solitons in sign-indefinite coupled nonlinear Schrödinger equations with a time-dependent harmonic trap, Commun. Nonlin. Sci. Numer. Simul. **31**, 30 (2016).

[46] Y. V. Kartashov and V. V. Konotop, Stable Nonlinear Modes Sustained by Gauge Fields, Phys. Rev. Lett. **125**, 054101 (2020).

[47] B. V. Gisin and A. A. Hardy, Stationary solutions of plane nonlinear-optical antiwaveguides, Opt. Quant. Electron **27**, 565 (1995).

[48] B. V. Gisin, A. Kaplan, and B. A. Malomed, Spontaneous symmetry breaking and switching in planar nonlinear optical antiwaveguides, Phys. Rev. E **62**, 2804 (2000).

[49] D. Bortman-Arbiv, A. D. Wilson-Gordon, and H. Friedmann, Strong parametric amplification by spatial soliton-induced cloning of transverse beam profiles in an all-optical antiwaveguide, Phys. Rev. A **63**, 031801(R) (2001).

[50] O. N. Verma and T. N. Dey, Steering, splitting, and cloning of an optical beam in a coherently driven Raman gain system, Phys. Rev. A **91**, 013820 (2015).

[51] A. Kaplan, B. V. Gisin, and B. A. Malomed, Stable propagation and all-optical switching in planar waveguide-antiwaveguide periodic structures, J. Opt. Soc. Am. B **19**, 522 (2002).

[52] H. Sakaguchi and B. A. Malomed, Dynamics of positive- and negative-mass solitons in optical lattices and inverted traps, J. Phys. B **37**, 1443 (2004).

[53] Y. Shin, G.-B. Jo, M. Saba, T. A. Pasquini, W. Ketterle, and D. E. Pritchard, Optical Weak Link Between Two Spatially Separated Bose-Einstein Condensates, Phys. Rev. Lett. **95**, 170402 (2005).

[54] S. J. Park, J. Noh, and J. Mun, Cold atomic beam from a two-dimensional magneto-optical trap with two-color pushing laser beams, Opt. Commun. **285**, 3950 (2012).

[55] H. Ma, A. K. Y. Jen, and L. R. Dalton, Polymer-based optical waveguides: Materials, processing, and devices, Adv. Mater. **14**, 1339 (2002).

[56] N. Hacker and B. A. Malomed, Nonlinear dynamics of wave packets in tunnel-coupled harmonic-oscillator traps, Symmetry **13**, 372 (2021).

[57] F. H. Stillinger and D. R. Herrick, Bound states in continuum, Phys. Rev. A **11**, 446 (1975).

[58] A. Kodigala, T. Lepetit, Q. Gu, B. Bahari, Y. Fainman, and B. Kante, Lasing action from photonic bound states in continuum, Nature **541**, 196 (2017).

[59] Y. V. Kartashov, V. V. Konotop, and L. Torner, Bound states in the continuum in spin-orbit-coupled atomic systems, Phys. Rev. A **96**, 033619 (2017).

[60] A. R. Champneys, B. A. Malomed, J. Yang, and D. J. Kaup, "Embedded solitons": Solitary waves in resonance with the linear spectrum, Physica D **152–153**, 340 (2001).

[61] Y. Guo, M. Xiao, and S. Fan, Topologically Protected Complete Polarization Conversion, Phys. Rev. Lett. **119**, 167401 (2017).

[62] B. Midya, and V. V. Konotop, Coherent-perfect-absorber and laser for bound states in a continuum, Opt. Lett. **43**, 607 (2018).

[63] L. Xu, K. Z. Kamali, L. Huang, M. Rahmani, A. Smirnov, R. Camacho-Morales, Y. X. Ma, G. Q. Zhang, M. Woolley, D. Neshev, and A. E. Miroshnichenko, Dynamic nonlinear image tuning through magnetic dipole quasi-BIC ultrathin resonators, Adv. Sci. **6**, 1802119 (2019).

[64] S. Romano, G. Zito, S. N. L. Yepez, S. Cabrini, E. Penzo, G. Coppola, I. Rendina, and V. Mocella, Tuning the exponential sensitivity of a bound-state-in-continuum optical sensor, Opt. Express **27**, 18776 (2019).

[65] B. A. Malomed, Vortex solitons: Old results and new perspectives, Physica D **399**, 108 (2019).

[66] A. Avila, Global theory of one-frequency Schrödinger operators, Acta Math. **215**, 1 (2015).

[67] B. A. Malomed, Variational methods in nonlinear fiber optics and related fields, Progr. Optics **43**, 71 (2002).

[68] L. D. Landau and E. M. Lifshitz, *Quantum Mechanics* (Nauka Publishers, Moscow, 1974).

[69] R. Nyden Hill, Rates of convergence and error estimation formulas for the Rayleigh-Ritz variational method, J. Chem. Phys. **83**, 1173 (1985).

[70] N. G. Vakhitov and A. A. Kolokolov, Stationary solutions of the wave equation in a medium with nonlinearity saturation, Radiophys. Quant. Electron. **16**, 783 (1973).

[71] L. Bergé, Wave collapse in physics: principles and applications to light and plasma waves, Phys. Rep. **303**, 259 (1998).

[72] G. Fibich, *The Nonlinear Schrödinger Equation: Singular Solutions and Optical Collapse* (Springer, Heidelberg, 2015).

[73] H. Sakaguchi and B. A. Malomed, Solitons in combined linear and nonlinear lattice potentials, Phys. Rev. A **81**, 013624 (2010).

[74] M. Quiroga-Teixeiro and H. Michinel, Stable azimuthal stationary state in quintic nonlinear optical media, J. Opt. Soc. Am. B **14**, 2004 (1997).

[75] L. D. Carr and C. W. Clark, Vortices in Attractive Bose-Einstein Condensates in Two Dimensions, Phys. Rev. Lett. **97**, 010403 (2006).

[76] Y. Li, Z. Chen, Z. Luo, C. Huang, H. Tan, W. Pang, and B. A. Malomed, Two-dimensional vortex quantum droplets, Phys. Rev. A **98**, 063602 (2018).

[77] M. R. Belić, A. Stepken, and F. Kaiser, Spatial Screening Solitons as Particles, Phys. Rev. Lett. **84**, 83 (2000).